Particle-in-cell simulations of tunneling ionization effects in plasma-based accelerators

David L. Bruhwiler,[a] D. A. Dimitrov,[a] John R. Cary,[a,b] Eric Esarey,[c]
Wim Leemans[c] and Rodolfo E. Giacone[b]

[a]Tech-X Corporation, 5541 Central Ave., Suite 135, Boulder CO 80301, USA
[b]University of Colorado, Physics Department, Boulder CO 80309-0390, USA
[c]Lawrence Berkeley National Laboratory, University of California, Berkeley CA 94720, USA

ABSTRACT

Plasma-based accelerators can sustain accelerating gradients on the order of 100 GV/m. If the plasma is not fully ionized, fields of this magnitude will ionize neutral atoms via electron tunnelling, which can completely change the dynamics of the plasma wake. Particle-in-cell simulations of a high-field plasma wakefield accelerator, using the OOPIC code [D.L. Bruhwiler *et al*., Phys. Rev. S.T. A&B, Issue 10 (2001)], which includes field-induced tunneling ionization of neutral Li gas, show that the presence of even moderate neutral gas density significantly degrades the quality of the wakefield. The tunneling ionization model in OOPIC has been validated via detailed comparison with experimental data from the l'OASIS laboratory [W.P. Leemans *et al*., Phys. Rev. Lett. **89**, 174802 (2002)]. The properties of a wake generated directly from a neutral gas are studied, showing that one can recover the peak fields of the fully ionized plasma simulations, if the density of the electron drive bunch is increased such that the bunch rapidly ionizes the gas.

PACS nos.: 41.75.Ht, 41.75.Lx, 52.25.Jm, 52.65.Pp, 52.65.Rr, 52.75.-d

I. INTRODUCTION

Plasma-based accelerators have demonstrated accelerating fields in excess of 100 GV/m (for a review, see Ref. [1]), which is two to three orders beyond that of conventional technology. The acceleration field in a plasma wakefield accelerator (PWFA)[2,3] is generated by a relativistic electron (or positron[4]) beam that is injected into a plasma. The self-fields of the drive bunch excite a wakefield, or electron plasma wave (EPW), that propagates behind with a group velocity close to the speed of light, *c*. According to linear theory,[5] the wakefield amplitude is maximum when $k_p\sigma_z \approx 2^{1/2}$, where σ_z is the rms bunch length, and $k_p=2\pi/\lambda_p$ is the plasma wavenumber. A trailing electron bunch can be accelerated by the longitudinal electric field and focused by the transverse electric field of the EPW.

Recent experiments (E-157 and E-162)[6-9] at the Stanford Linear Accelerator Center (SLAC) have studied the physics of the PWFA in the nonlinear "blowout" regime[10] using a 30 GeV electron beam in a meter-long plasma. In these experiments, the plasma was produced by partially ionizing (roughly 10%) the neutral gas in a Li oven, using a long focal length UV-laser (193 nm). By enhancing the drive electron beam and plasma parameters, the PWFA has been proposed[11] as a method for doubling the beam energy of the Stanford Linear Collider (SLC), or some future linear electron-positron collider, in a distance of order ten meters, with an average accelerating gradient of roughly 10 GV/m and peak fields on the order of 30 GV/m. This "plasma afterburner" could potentially enable detection of the Higgs particle at the SLC.

We present 2-D particle-in-cell (PIC) simulations of PWFA configurations relevant to the plasma afterburner concept. These simulations are conducted using the code OOPIC,[12,13] which includes the physics of tunneling ionization. There have been many contributions to the quasi-classical calculation of tunneling ionization probability rates in atoms and ions,[14-18] as well as some controversy regarding precedence.[19] The probability rate implemented in OOPIC is taken from Eq. (1) of Ref. [17], which we refer to as the Ammosov-Delone-Krainov (ADK) model. Our results show that field ionization has a dramatic impact on the dynamics of the EPW. The

ADK model in OOPIC has been validated via direct comparison with experimental data from the l'OASIS laboratory[20] of Lawrence Berkeley National Laboratory (LBNL).

In Sec. II, we briefly discuss the ADK model and ionization probability rates. In Sec. III, we present comparisons to experiments on ionization-induced blue shifting of laser pulses. In Sec. IV, we discuss the baseline case of a PWFA with no tunneling ionization. We then show in Sec. V that the electric fields of the drive beam and the EPW will fully ionize much of the background Li gas. If the gas is only 10% pre-ionized, as in the case of the E-157 and E-162 experiments, then the wake is completely disrupted. Finally, in Sec.'s VI and VII, we show that the drive beam can simultaneously ionize the plasma and create a strong EPW, but only if the beam density is increased sufficiently. Our conclusions are presented in Sec. VIII.

II. THE ADK TUNNELING IONIZATION MODEL

A number of formulae for the field-induced ionization rate of ions and neutral atoms have been derived theoretically. Several of these analytical models have been recently summarized by Bauer and Mulsner,[21] who compared them with a numerical solution of the time-dependent Schrödinger equation (TDSE) for an electron in a Coulomb potential with a superimposed external electric field E(t). Their analysis shows that the ADK formula for Hydrogen agrees well with numerical solutions of the TDSE, for magnitudes of the external electric field no larger than the critical value: [22]

$$E_{crit} = \left(\sqrt{2} - 1\right)\left|\xi_i\right|^{3/2} \qquad \text{Eq. (1)}$$

where ξ_i is the energy of the electron's unperturbed ground state, from which the transition to the unbound state occurs.

Eq. (1) is presented in scaled atomic units. In Eq. (1), E_{crit} is normalized to the atomic field $E_a=\kappa^3 m_e^2 e^5/\hbar^4 \approx 5.14 \times 10^{11}$ V/m, while ξ_i is normalized to the atomic energy scale

$\xi_a=\kappa^2 m_e e^4/\hbar^2 \approx 4.36\text{x}10^{-18}$ J (or ≈27.2 eV). We use MKS units for unscaled quantities, such as Planck's constant, the electron mass m_e, and electron charge e. Further, we use $\kappa=1/4\pi\varepsilon_0$, where ε_0 is the permittivity of free space.

For very strong external electric fields, such that $E>E_{crit}$, the ionizing mechanism is not tunneling, but barrier suppression ionization (BSI). It has been shown[21] that a simple BSI model can be effectively patched with a tunneling model, like ADK, yielding a combined model that works well for a broad range of electric field amplitudes. Other work[23] has shown that the ADK model yields better agreement with experimental data than do other tunneling models. In the present work, we primarily consider field-induced ionization of neutral Li by electric fields smaller than $E_{crit}\approx 18.7$ GV/m, thus we do not use a BSI model.

The ADK probability rate for tunneling ionization of the outermost electron from its ground state energy level (with orbital quantum number l and its projection m assumed to be zero) in an atom or ion, is given in atomic units by Eq. (2).

$$W_a(E)=\frac{4^{n^*}\xi_i}{n^*\Gamma(2n^*)}\left(\frac{2\xi_0}{E}\right)^{2n^*-1}\exp\left(-\frac{2\xi_0}{3E}\right) \qquad \text{Eq. (2)}$$

Here, W_a is normalized to the inverse of the atomic time interval $\tau_a=\hbar^3/m_e e^4\kappa^2\approx 2.42\text{x}10^{-17}$ s. A value of unity would indicate 100% ionization during a time τ_a, if the electric field magnitude were constant during that interval. Also, $\xi_0=(2\xi_i)^{2/3}$ is a dimensionless parameter, and Γ is the standard Gamma function. The "effective" principal quantum number[17] is defined to be $n^*\equiv Z/(2\xi_i)^{1/2}$, where Z is the charge number for the ion after ionization (i.e. Z=1 for ionization of a neutral atom).

Eq. (2) is quasistatic result, which assumes that the external electric field changes slowly compared to time scales of interest. Ref. [17] emphasizes a time-averaged variation of Eq. (2), which would be appropriate for simulations of linearly polarized electromagnetic fields that use an envelope approximation (i.e. do not time resolve the high-frequency oscillations). For time-

explicit PIC codes like OOPIC, the quasistatic formula is appropriate, because any time variation of the electric fields is fully resolved.

Another subtle issue regarding the ADK tunneling ionization rate formula arises from the use of Stirling's formula to approximate the Gamma function Γ. Two Gamma functions arise in the calculation of the coefficients $C_{n^*l^*}$ in Ref. [17], where they are replaced (without any discussion) by only the first term of the well-known Stirling expansion. It has been noted[19] that this unnecessary approximation causes an error that exceeds 10% in the ionization rates for H and He. In Eq. (2), we have used the assumption that the effective orbital quantum number for atoms and ions in the ground state has the form l*=n*-1 (from Eq. (17) in Ref. [17]), allowing us to present the ionization rate formula with only a single Gamma function.

We now recast Eq. (2) into a more convenient form, where the ionization probability rate is shown to depend only on the local electric field magnitude (in units of GV/m) and the ionization energy (in units of eV) of the atom or ion.

$$W\left[s^{-1}\right] \approx 1.52x10^{15} \frac{4^{n^*}\xi_i[eV]}{n^*\Gamma(2n^*)}\left(20.5\frac{\xi_i^{3/2}[eV]}{E[GV/m]}\right)^{2n^*-1}\exp\left(-6.83\frac{\xi_i^{3/2}[eV]}{E[GV/m]}\right) \quad \text{Eq. (3)}$$

Likewise, the effective principal quantum number can be written in the form $n^* \approx 3.69Z/\xi_i^{1/2}[eV]$. Eq. (3) is an approximation to the model implemented in the OOPIC code.

For gas densities of order 10^{19} cm^{-3} or less, there is no need to explicitly account for the field energy required to ionize the atoms or ions, because the energy extracted from the fields via the standard PIC algorithm, due to acceleration of the electrons during the first time step after ionization, is much larger than the ionization energy. The code issues a warning to the user if the total ionization energy exceeds a small fraction of the local field energy in a grid cell. For much higher densities, it would be necessary to treat this issue more carefully, by adding a polarization current,[24-26] which would correctly decrement the electric field during the same time step in which the electrons are ionized.

We now consider the specific case of Li. Table I shows the ionization energy, the residual charge number, the effective principal quantum number and the critical electric field for Li and Li+. The same information for H, He, He+, Cs and Cs+ is presented in Table I for the sake of comparison. Using the values of ξ_i and n* for neutral Li, we can recast Eq. (2) into a simpler form that is specific to tunneling ionization of Li.

$$W_{Li}\left[s^{-1}\right] \approx \frac{3.60x10^{21}}{E^{2.18}\left[GV/m\right]} \exp\left(\frac{-85.5.}{E\left[GV/m\right]}\right) \qquad \text{Eq. (4)}$$

Eq. (4) presents the ionization rate for Li->Li+, as a function of the local electric field magnitude in GV/m. For a time interval Δt, during which the field magnitude is constant, the fraction of neutral Li atoms in the local area that are ionized during this interval is given by $F_{Li} \approx W_{Li} \Delta t$.

Eq. (4) can be used to estimate the relevance of tunneling ionization physics to present and future PWFA experiments. We consider a relativistic drive beam of electrons with an rms length of $\sigma_z \approx 100$ μm and a total length of $L \approx 6\,\sigma_z$, which corresponds to a transit time of approximately $2x10^{-12}$ s. We further suppose that a PIC simulation of this beam would use a grid spacing on the order of 10 μm, with a time step on the order of $2x10^{-14}$ s.

Fig. 1 shows $F_{Li} \approx W_{Li} \Delta t$, the fractional ionization for neutral Li, during a single time step (solid curve) and during a beam transit time (dashed curve), as a function of peak electric field. The dashed curve provides only very rough guidance, because the fields vary from zero to their peak value during a beam transit. In contrast, the solid curve is fairly accurate, because the local electric field does not change significantly during a single time step of the PIC algorithm.

Examination of Fig. 1 leads to two conclusions for PWFA experiments using Li: 1) tunneling ionization becomes a concern when the peak fields exceed 4 GV/m, and 2) there will be 100% ionization of the local Li gas in a single PIC time step when the local fields exceed 6 GV/m. The rms length of the drive beam for the proposed afterburner would be significantly shorter (~60 μm) than that for the E-157 and E-162 experiments (~600 μm), but our conclusions

are insensitive to this difference. Rather, our conclusions are dominated by the exponential dependence of the ionization probability rate on the local electric field magnitude. Thus, we conclude that tunneling ionization is irrelevant to the previous E-157 and E-162 experiments, where the peak fields were of order 1 GV/m, but will dominate the wake dynamics for future high-field experiments such as the plasma afterburner, where peak fields on the order of 30 GV/m are expected.

We now briefly consider two related issues: 1) will field-induced ionization of Li+ be a concern for afterburner parameters, and 2) could other gasses be used for future high-field PWFA experiments? Both of these issues are directly addressed by Fig. 2, which shows the fractional ionization during a single PIC time step for Li, Li+, Cs, Cs+, H and He. The right-most curve of Fig. 2 shows that ionization of Li+ is not a concern, unless the peak electric fields exceed 200 GV/m, which will not occur for expected parameters of the proposed plasma afterburner.

Comparison of the left-most curve in Fig. 2 (solid, for Cs) with the neighboring curve (dashed, for Li) shows that the electric field amplitudes required to ionize Cs are almost half as large as those required for Li. The fourth curve from the left (dash-dot), shows that ionization of Cs+ becomes a concern for peak electric fields exceeding 40 GV/m, which could certainly occur for afterburner parameters. Thus, Cs is an interesting candidate for use in future PWFA experiments.

It would be attractive for future PWFA experiments to use gasses like H or He, rather than Li or Cs. The third curve from the left (dotted) in Fig. 2, shows that electric fields on the order of 30 GV/m are required to quickly ionize H. The second curve from the right (dash-dot-dot) shows that fields on the order of 90 GV/m are required to quickly ionize He. Thus, one could only use H or He for very high-field PWFA experiments.

III. IONIZATION INDUCED FREQUENCY SHIFTS

To test the validity of the ADK tunneling ionization model in the code OOPIC, comparisons were made to experiments of the l'OASIS Group at LBNL on the ionization-induced frequency shifts in an ultra-short laser pulse traversing a gas plume (mm scale length) from a nozzle of a pulsed jet. In many cases, a laser pulse in LWFA (laser wakefield accelerator) experiments must create its own plasma via field-induced tunneling ionization of a neutral gas. Tunneling ionization due to laser pulse propagation in a neutral gas leads to frequency up-shifting (blue shifting) of the laser pulse as it propagates through the gas, as has been observed and analyzed by several groups[27,28]. A nonlinear expression for the frequency upshift has been derived analytically.[29] Recently, Leemans *et al.* have proposed and used ionization-induced blue shifting as a method for determining optimized compression of the laser pulses in a chirped-pulse amplification laser system.[20,30]

The tunneling ionization has important ramifications to the intensively studied LWFA concept. In particular, the leading edge of the laser pulse can steepen due to ionization-induced pump depletion, which can seed and enhance the self-modulation instability.[31] Also, electron density gradients in the transverse wings of the pulse refract some energy away and modify the transverse profile via ionization induced refraction.[32]

The tunneling ionization model implemented in the OOPIC code has been validated for He and He+ via detailed comparisons with experimental data from the l'OASIS laboratory of LBNL. In particular, the blue shifting of the spectrum of a Gaussian laser pulse due to ionization of a neutral He gas jet has been examined via FFT's of the simulated laser pulse and compared with the output of a laboratory spectrometer.[33]

A He gas jet with a Gaussian profile is used in the experiments. Its width is 3 mm, which is approximately 22 Rayleigh lengths. The maximum gas density is 2×10^{19} cm^{-3} leading to a peak plasma density of 4×10^{19} cm^{-3}. The laser pulse is linearly polarized with a Gaussian profile, both transversely and longitudinally. The experiments considered here used moderate intensity

laser pulses, with a total energy of 20.5 mJ and full width at half maximum (FWHM) pulse lengths between 50 and 200 fs. The laser wavelength λ is 800 nm, the frequency is 2.355×10^{15} rad/s, the waist size is 6 μm with the Rayleigh length approximately $R_L \approx 141$ μm in vacuum.

We conducted 2D simulations in *x*-*y* slab geometry with *x* as the longitudinal direction, the direction of propagation of the laser pulse. The polarization of the pulse is along *z*, the ignorable coordinate. The pulse is launched from the left boundary (constant value of *y*) of the simulation box and propagates to the right. The description of how laser pulses are launched in OOPIC is given by Bruhwiler *et al.* [13].

OOPIC has a moving window algorithm that enables propagation of the laser pulse over a distance greater than the longitudinal length of the simulation box. The laser pulse in the simulations has a Gaussian profile along the transverse directions and a half-sine along the direction of propagation. The half-sine along *x* differs from the shape of the pulse in the experiments, but this choice was made to keep the simulation box of manageable size, both in terms of available CPU time and memory.

The longitudinal and transverse grid sizes are respectively $dx = 0.05$ μm and $dy = 0.8$ μm. This leads to a spatial resolution of 16 (λ/dx). The Courant condition must be satisfied by the time step, leading to $dt = 1.2\times10^{-16}$ s and time resolution of $1/(\nu dt) = 31$. We did runs with 50, 100, and 200 fs FWHM pulse lengths. The grid length along *x* is chosen large enough to provide containment of the laser pulses and not to introduce any significant boundary effects. Simulations were done with a number of grid cells $N_x = 1024$, 1536, 3072 along *x* and $N_y = 1024$ along *y*.

The pulse is initially launched in vacuum and propagated for approximately one longitudinal grid length L_x, until it is completely contained in the simulation box. Then the laser pulse enters the domain of the He gas. The gas profile is a linear ramp increasing in a small number of grid cells along *x* from zero to a constant gas density equal to the maximum gas

density of the experiments. Once the maximum gas density is reached, it is then kept constant for the rest of the simulations.

The pulse is propagated for twelve Rayleigh lengths, which corresponds to the same integrated gas density as in the experiments. Propagating the laser pulses half the distance through the peak gas density helps to keep memory requirements and CPU times to manageable levels, but this approach leads to some important differences, such as self-modulation of the pulses. For each simulation, the integrated power spectrum of E_z is calculated via FFT, resulting in spectra similar to those measured experimentally.[33] We define the 10% blue-shift wavelength to be the wavelength at which the power spectrum first reaches 10% of the 800 nm peak value, when moving from the high frequency (short wavelength) part of the spectrum toward the peak.

Fig. 3 shows our simulated 10% blue-shift wavelength (squares) together with experimental measurements (triangles). The simulation results show good agreement with the data. This quantitative agreement provides confidence in the implementation of the ADK model within OOPIC.

IV. PWFA WITHOUT TUNNELING IONIZATION

In the following sections, the results of OOPIC simulations in 2-D cylindrical geometry are presented for a PWFA with parameters relevant to the plasma afterburner concept. The 50 GeV electron drive beam, shown in Fig. 4a, has a Gaussian distribution with rms radius σ_r=20 μm and length σ_z=63 μm (compared to σ_r=35 μm and σ_z=600 μm in typical E-157 experiments). The total beam length, L=6σ_z, is slightly larger than the plasma wavelength, λ_p=282 μm, which corresponds to a plasma density n_e=1.4x10^{16} cm^{-3} (approximately 100 times higher density than in the E157 experiments). The spatial dimensions in Fig. 4 are normalized to λ_p. The grid size is Δz=Δr=7.5 μm. Roughly 34,000 macro-particles are used to represent the beam, for an average of 80 particles per cell.

A "moving window" algorithm enables the simulation to follow the electron beam for long times, while using a grid that is just large enough to model the beam and the following EPW. This algorithm follows the rightward propagating beam by shifting all particles and fields one grid cell to the left at time intervals that are chosen to track features moving at the speed of light, *c* [see Ref. 13 for details].

Fig. 4b shows the nonlinear plasma wake or EPW, which is driven by the self-fields of the 50 GeV electron drive beam in a fully pre-ionized plasma. The wake is approximately periodic with period near λ_p. Roughly 56,000 macro-particles are used to represent the plasma, corresponding to seven particles per cell. Cold electrons are injected from the right boundary, as the moving window algorithm follows the drive beam. Particles are removed at the left boundary, which is also a perfect sink for fields.

The beam macro-particles represent $2x10^{10}$ physical electrons, which is consistent with typical parameters for the SLC. Given the rms sizes specified above, this corresponds to a peak number density of $n_b=1.0x10^{17}$ cm^{-3} (approximately 30 times higher density than in the E-157 experiments). The peak beam density exceeds the plasma density, which corresponds to the "blow-out regime", where plasma electrons are blown completely off-axis (cavitate) and then coalesce into a very small volume behind the drive beam. This physical picture is shown in Fig.'s 4a and 4b.

The extremely large electron density on axis, where the plasma electrons coalesce immediately behind the blowout region, leads to a correspondingly large longitudinal electric field component, E_z. The surface plot of E_z in Fig. 4c shows strong localized peaks on the r=0 axis, spatially separated by λ_p. The field is normalized to the cold, nonrelativistic wavebreaking field $E_p=m_e c^2 k_p/e=11.4$ GV/m, where $k_p=2\pi/\lambda_p$.

The fields exceed E_p, consistent with the nonlinear dynamics of the blow-out regime, with a peak value of -16.5 GV/m. The lineout of E_z along r=0, presented in Fig. 4d, shows more clearly the periodicity and the peak values. The magnitude of the peaks is seen to decrease with

distance from the drive beam, corresponding to a loss of coherence in the plasma wake over time.

V. PWFA WITH TUNNELING IONIZATION IN A PARTIALLY PRE-IONIZED GAS

The plasma source in the E-157 and E-162 experiments[6-8] at SLAC was based on a Li oven in which the Li gas was 10% pre-ionized using a long focal length laser. Given a pre-ionized plasma density of 1.4×10^{16} cm^{-3} for the proposed afterburner, this implies a neutral Li density of 1.26×10^{17} cm^{-3}. We now consider simulations of this scenario, using the same drive beam parameters, with tunneling ionization effects included, and find that the plasma wake is severely disrupted. Here the tunneling ionization is due to the large space charge field associated with the high density electron bunch.

In Fig. 5a, which shows the plasma wake, the spatial dimensions are normalized to λ_p=89 μm, corresponding to a total plasma density $n_e=1.4 \times 10^{17}$ cm^{-3}. The pre-ionized plasma is represented by seven macro-particles per cell. Up to 27 Li^+/e^- pairs are created in each cell where tunneling ionization of the neutral Li occurs.

Fig. 5b shows the corresponding lineout of the longitudinal electric field E_z along r=0, zooming in on the region near the drive beam. E_z shows periodicity with the new shorter plasma wavelength, which is physically correct. The field is normalized to the new, larger wavebreaking field E_p=36.1 GV/m. The peak fields are smaller than E_p, showing a linear plasma response, which is consistent with the fact that the peak beam density is now smaller than the plasma density. We note, however, that the peak field in physical units is approximately 13 GV/m, which is not very different from the peak fields for the ideal case shown in Fig. 4.

We note that electron-impact ionization (by the drive beam and by electrons in the wake) and electron-neutral scattering can play an important physical role in beam-plasma interactions. The OOPIC code includes relativistic impact and scattering algorithms,[13] which have been used

to simulate the afterburner concept (with parameters very close to those used in this section, but in the absence of tunneling ionization) and also to model a plasma lens experiment.[34] These afterburner simulations showed that impact ionization and scattering by plasma electrons did not significantly modify the plasma wake. However, impact ionization by the beam electrons created secondary electrons within the blowout region, which were all trapped and quickly accelerated to very high energies.

Because the effects of tunneling ionization are so strong in this regime, it is unclear how important self-trapping due to impact ionization will be. We have not yet done a careful study of PIC simulations with both tunneling and impact ionization included. However, the issue of self-trapping in future PWFA experiments is very important and merits further exploration.

VI. PWFA WITH TUNNELING IONIZATION IN A NEUTRAL GAS

The results of the previous section show that the electric fields of the drive beam are large enough to ionize the neutral Li gas, which is consistent with the analysis presented in Sec. II above. Hence, it may be unnecessary to pre-ionize the Li, which would greatly reduce the cost and complexity of future high-field PWFA experiments. We now consider this possibility.

Simulations using the same drive beam parameters described above, with a neutral Li density of 1.4×10^{16} cm^{-3} and no pre-ionized plasma, show significant ionization of the gas, but the resulting wake generated by the secondary electrons is incoherent. The wake is shown in Fig. 6a. Up to 27 Li^+/e^- pairs are created in each cell where tunneling ionization of the neutral Li occurs. Fig. 6b shows a lineout of the longitudinal electric field E_z along r=0. The field is normalized to the same wavebreaking field used in Fig. 4, E_p=11.4 GV/m. The fields do not exceed E_p, indicating a linear plasma response, because the electrons are not created quickly enough through ionization to respond resonantly to the drive beam.

VII. PWFA WITH HIGHER-DENSITY DRIVE BEAM AND NEUTRAL GAS

The results of the previous section suggest that it is important to ionize the Li gas as quickly as possible. This can only be accomplished by increasing the self-fields of the beam, which implies that one must increase the number density of electrons in the beam. The number density can be raised by increasing the total number of electrons or by decreasing the physical dimensions σ_r and σ_z.

We now consider a 50 GeV electron drive beam, containing $2x10^{10}$ electrons in a Gaussian distribution with rms radius σ_r=10 μm and length σ_z=30 μm, which implies a peak number density of $n_b=8.5x10^{17}$ cm^{-3}. Fig. 7a shows the resulting plasma wake, which is considerably less structured than the idealized wake shown in Fig. 4b and also decoheres much more quickly.

Fig. 7b shows a lineout of E_z along r=0, for which one sees that the initial peak value is very nearly as large as is shown in Fig. 4d for the ideal case. The field is normalized to the cold, nonrelativistic wavebreaking field E_p=11.4 GV/m. The fields exceed E_p, showing an initially nonlinear plasma response.

Subsequent peaks in E_z decrease rapidly with distance from the electron drive beam, but this is not important, for the following reason. In the plasma afterburner concept, the witness beam and the drive beam will be created from the same initial electron bunch and will follow closely in time such that the witness beam is accelerated by the first electric field peak of the wake from the drive beam. In the present work, we consider only the drive beam, but the witness beam would be located just in front of the first peak in E_z. Thus, the simulation results presented in Fig. 7 suggest very strongly that future PWFA experiments could dispense with pre-ionization of the Li gas, if the number density of the drive bunch can be made sufficiently large.

The above results on the PWFA have been concerned with the case of the blow-out regime for intense electron beam drivers. In electron-positron collider applications, it would be very beneficial if large amplitude wakefields could also be generated with positron beam drivers.

Positron beam driven wakefields have been simulated,[4] neglecting the effects of ionization. This work showed that, for an initially homogenous plasma, nonlinear positron wakes are smaller than corresponding electron wakes due to the fact that the plasma electrons are "sucked-in" for positron drivers (as opposed to blown-out for electron drivers).

It was shown in Ref. [4] that hollow plasma channels can enhance the amplitude of the positron wakes. It was further suggested that a hollow plasma channel can be made by UV ionization of a long gas column by a laser for which the center is blocked. This method, however, would result in a plasma channel in which the center is filled with neutral gas. Given the results presented here, such a channel would be unacceptable for intense positron drivers for which tunneling ionization would occur.

VIII. CONCLUSION

The code OOPIC has been upgraded to include both field and particle induced ionization effects. In the case of field induced ionization by an intense laser, the code has been benchmarked against experiments[20] conducted at the l'OASIS facility. The spectra of ionization induced blue-shifting of an intense laser beam propagating through an initially neutral Helium gas was computed and found to compare very well[33] with experimentally measured spectra.

We have shown for the first time that field-induced tunneling ionization is a critically important effect in proposed high-field PWFA experiments such as the plasma afterburner concept. Our results show that one must operate in one of two regimes in order to obtain a high-quality plasma wake: work with a 100% pre-ionized plasma and negligible background neutral gas, or else work with neutral gas only and increase the peak number density of beam electrons to the point where the drive beam can simultaneously ionize the gas and generate a strong wake.

The first approach is not practical, because it is very difficult to reliably generate a 100% ionized plasma over a distance of several meters, as would be required for the afterburner concept. The second approach increases the burden on the linear accelerator producing the drive bunch, but it has the excellent benefit of removing the need for a laser system to pre-ionize the

gas. This exciting result, which emerged from numerical simulations using the 2-D PIC code OOPIC, shows how to reduce the cost and complexity of future high-field PWFA experiments.

These results strongly suggest important areas for future work. The long-time evolution of electron and positron beam drivers for future PWFA experiments must be simulated, in order to understand how tunneling ionization will erode the leading edge of such beams. The radial electric field of the plasma wake can very tightly compress a drive beam in the radial direction, which in turn will greatly increase the self-fields of the beam. Thus, it may be possible to pre-ionize only the leading edge of a long gas cell for PWFA experiments, in such a way that the drive beam will be compressed to the point that it can then self-ionize the neutral gas for the remaining length of the gas cell. This concept merits study. Also, the general problem of how tunneling ionization effects modify the wake generated by positron beam drivers should be simulated. Finally, the differences between tunneling ionization in Cs, rather than Li, should also be explored.

IX. ACKNOWLEDGEMENTS

The authors gratefully acknowledge helpful conversations with D. Abell, C. Birdsall, B. Blue, R. Busby, P. Catravas, P. Chen, C. Clayton, S. Deng, D. Gordon, B. Hafizi, M. Hogan, R. Hubbard, C. Joshi, G. Joyce, T. Katsouleas, K. Luetkemeyer, P. Mardahl, K. Marsh, W. Mori, P. Muggli, J. Ng, B. Shadwick, G. Shvets, P. Stoltz, F. Tsung, Cs. Toth, D. Umstadter, J. Verboncoeur and J. Wurtele. Comments from an anonymous referee were also very helpful. This work is supported in part by the SciDAC project -- Advanced Computing for 21st Century Accelerator Science & Technology, an initiative of the U.S. Department of Energy, under Contract No. DE-FG02-01ER41178. This work is further supported by the U.S. Department of Energy, under Contract No.'s DE-FG03-99ER82903, DE-FG03-20ER83557, DE-FG03-95ER40926 and DE-AC03-76SF00098, and by Tech-X Corporation. This work used resources of the National Energy Research Scientific Computing Center.

X. REFERENCES

1. E. Esarey, P. Sprangle, J. Krall and A. Ting, IEEE Trans. Plasma Sci. **24**, 252 (1996).
2. P. Chen, J. Dawson, R. Huff and T. Katsouleas, Phys. Rev. Lett. **54**, 693 (1985).
3. R. Ruth, A. Chao, P. Morton, and P. Wilson, Part. Accel. **17**, 171 (1985).
4. S. Lee, T. Katsouleas, R.G. Hemker, E.S. Dodd and W.B. Mori, Phys. Rev. E **64**, 045501 (2001).
5. R. Keinigs and M.E. Jones, Phys. Fluids **30**, 252 (1987)
6. M.J. Hogan, R. Assmann, F.J. Decker, R. Iverson, P. Raimondi, S. Rokni, R.H. Siemann, D. Walz, D. Whittum, B. Blue, C.E. Clayton, E. Dodd, R. Hemker, C. Joshi, K.A. Marsh, W.B. Mori, S. Wang,T. Katsouleas, S. Lee, P. Muggli, P. Catravas, S. Chattopadhyay, E. Esarey, and W.P. Leemans, Phys. Plasmas **7**, 2241 (2000).
7. P. Catravas, W.P. Leemans, S. Chattopadhyay, E. Esarey, R. Assmann, F.J. Decker, A. Geraci, R. Iverson, M.J. Hogan, S. Rokni, R.H. Siemann, D. Walz, D. Whittum, B. Blue, C. Clayton, C. Joshi, K. Marsh, W.B. Mori, S. Wang, T. Katsouleas, S. Lee, and P. Muggli, Phys. Rev. E **64**, 046502, (2001).
8. C.E. Clayton, B.E. Blue, E.S. Dodd, C. Joshi, K.A. Marsh, W.B. Mori, S. Wang, P. Catravas, S. Chattopadhyay, E. Esarey, W.P. Leemans, R. Assmann, F.J. Decker, M.J. Hogan, R. Iverson, P. Raimondi, R.H. Siemann, D. Walz, T. Katsouleas, S. Lee, and P. Muggli, Phys. Rev. Lett. **88**, 154801 (2002).
9. C. Joshi, B. Blue, C.E. Clayton, E. Dodd, C. Huang, K.A. Marsh, W.B. Mori, S. Wang, M.J. Hogan, C. O'Connell, R. Siemann, D. Watz, P. Muggli, T. Katsouleas and S. Lee, Phys. Plasmas **9**, 1845 (2002).
10. J.B. Rosenzweig, B. Breizman, T. Katsoulaeas, and J.J. Su, Phys. Rev. A 44, 6189 (1991).

11. S. Lee, T. Katsouleas, P. Muggli, W.B. Mori, C. Joshi, R. Hemker, E.S. Dodd, C.E. Clayton, K.A. Marsh, B. Blue, S. Wang, R. Assmann, F.J. Decker, M. Hogan, R. Iverson and D. Walz, Phys. Rev. ST Accel. Beams **5**, 011001 (2002).
12. J.P. Verboncoeur, A.B. Langdon and N.T. Gladd, Comp. Phys. Comm. **87**, 199 (1995).
13. D.L. Bruhwiler, R.E. Giacone, J.R. Cary, J.P. Verboncoeur, P. Mardahl, E. Esarey, W.P. Leemans and B.A. Shadwick, Phys. Rev. S.T. A&B **4**, 101302 (2001).
14. L.V. Keldish, Sov. Phys. JETP **20**, 1307 (1965).
15. A.I. Nikishov and V.I. Ritus, Zh. Eksp. Teor. Fiz. **50**, 255 (1966) [Sov. Phys. JETP **23**, 162 (1966).].
16. A.M. Perelomov, V.S. Popov, M.V. Terent'ev, Zh. Eksp. Teor. Fiz. **50**, 1393 (1966) [Sov. Phys. JETP **23**, 943 (1966)].
17. M.V. Ammosov, N.B. Delone and V.P. Krainov, Sov. Phys. JETP **64**, 1191 (1986).
18. N.B. Delone and V.P. Krainov, Multiphoton Processes in Atoms, 2nd ed. (Springer, 1999).
19. V.S. Popov, Usp. Fiz. Nauk **169**, 819 (1999) [Phys. Uspekhi **42**, 733 (1999)].
20. W.P. Leemans, P. Catravas, E. Esarey, C.G.R. Geddes, C.T.R. Trines, C.B. Schroeder, B.A. Shadwick, J. van Tilborg and J. Faure, Phys. Rev. Lett. **89**, 174802 (2002); W.P. Leemans, D. Rodgers, P.E. Catravas, C.G.R. Geddes, G. Fubiani, E. Esarey, B.A. Shadwick, R. Donahue and A. Smith, Phys. Plasmas **8**, 2510 (2001).
21. D. Bauer and P. Mulser, Phys. Rev. A **59**, 569 (1999).
22. D. Bauer, Phys. Rev. A **55**, 2180 (1997).
23. S. Augst, D.D. Meyerhofer, D. Strickland and S.L. Chin, J. Opt. Soc. Am. B **8**, 858 (1991).
24. P. Mulser, F. Cornolti, and D. Bauer, *Phys. Plasmas* **5**, 4466 (1998).
25. S.C. Rae and K. Burnett, *Phys. Rev. A* **46**, 1084 (1992).

26. F. Cornolti, A. Macchi and E.C. Jarque, in *Superstrong Fields in Plasmas, Proceedings of the First International Conference*, eds. M. Lontano *et al*., AIP Conf. Proc. **426** (AIP, New York, 1998), pp. 55-60.
27. P.B. Corkum, IEEE J. Quantum Electron. **21**, 216 (1985).
28. W.M. Wood, G. Focht and M. Downer, Opt. Lett. **13**, 984 (1988).
29. E. Esarey, G. Joyce, and P. Sprangle, Phys. Rev. A **44**, 3908–3911 (1991).
30. W.P. Leemans, D. Rodgers, P.E. Catravas, G. Fubiani, C.G.R. Geddes, E. Esarey, B.A. Shadwick, G.J.H. Brussaard, J. van Tilborg, S. Chattopadhyay, J.S. Wurtele, L. Archambault, M.R. Dickinson, S. DiMaggio, R. Short, K.L. Barat, R. Donahue, J. Floyd, A. Smith and E. Wong, Advanced Accelerator Concepts, AIP Conf. Proc. **569**, edited by P.L. Colestock and S. Kelly (American Institute of Physics, Melville NY, 2001), p. 136.
31. D.L. Fisher and T. Tajima, Phys. Rev. E **53**, 1844-1851 (1996); D. Gordon *et al*., Phys. Rev. E **64**, 046404 (2001).
32. W.P. Leemans, C.E. Clayton, W.B. Mori, K.A. Marsh, P.K. Kaw, A. Dyson, C. Joshi and J.M. Wallace, Phys. Rev. A **46**, 1091-1105 (1992).
33. D.A. Dimitrov, D.L. Bruhwiler, W.P. Leemans, E. Esarey, P. Catravas, Cs. Toth, B.A. Shadwick, J.R. Cary and R. Giacone, Advanced Accelerator Concepts, AIP Conf. Proc. **647**, edited by C.E. Clayton and P. Muggli (American Institute of Physics, Melville NY, 2002), p. 192.
34. D.L. Bruhwiler, P. Chen, J. Ng, W. Leemans, E. Esarey, J.R. Cary and R. Giacone, Bull. Am. Phys. Soc. **45**, No. 7, p. 27 (2000).

XI. TABLES

Table I. Ionization energy and related quantities for H, He, Li and Cs

Atom/Ion	ξ_i [eV]	Z	n*	E_{crit} [GV/m]
H	13.6	1	1.00	75.3
He	24.5	1	0.746	182.
He+	54.4	2	1.00	602.
Li	5.39	1	1.59	18.7
Li+	75.5	2	0.848	985.
Cs	3.89	1	1.87	11.5
Cs+	25.1	2	1.47	189.

XII. FIGURE CAPTIONS

Fig. 1. The fractional ionization for neutral Li, during a single PIC time step (solid curve) and during a beam transit time (dashed curve), is shown as a function of peak electric field for an electron drive beam with rms length 100 μm. These results, obtained from Eq. (4), show that tunneling ionization of background neutral Li gas will be a key physical effect for PWFA experiments with peak electric fields on the order of 4 GV/m or larger.

Fig. 2. Curves showing the fractional ionization during a single PIC time step for (from left to right) Cs (solid), Li (dashed), H (dotted), Cs+ (dash-dot), He (dash-dot-dot) and Li+ (hashed), as a function of peak electric field. These results were obtained from Eq. (3) and Table I.

Fig. 3. The 10% blue-shift wavelength (see text), as a function of laser pulse length (for fixed pulse energy), is shown as simulated by the OOPIC code (squares) and as measured at the l'OASIS laboratory (triangles).

Fig. 4a. The 50 GeV e^- drive beam, shown here in cylindrical geometry, has a Gaussian distribution with RMS radius σ_r=20 μm and length σ_z=63 μm, with a total length L=6σ_z of approximately one plasma wavelength λ_p. The spatial dimensions are normalized to λ_p=282 μm, corresponding to plasma density $n_e=1.4\text{x}10^{16}$ cm^{-3}. The grid size is $\Delta z=\Delta r$=7.5 μm. Roughly 34,000 particles are used, for an average of 80 particles per cell.

Fig. 4b. The nonlinear plasma wake, driven by the self-fields of the 50 GeV e^- drive beam, is approximately periodic, with a period equal to the plasma wavelength λ_p. Roughly 56,000 particles are used, corresponding to seven particles per cell. A cold e^- plasma is injected from the right boundary, as the moving window algorithm follows the drive beam, which propagates at the speed of light c. Particles are removed at the left boundary.

Fig. 4c. This surface plot of the longitudinal electric field E_z, due to both the electron beam and the resulting plasma wake (but dominated by the wake), shows strong localized peaks on the r=0 axis, spatially separated by λ_p. The field is normalized to the cold, nonrelativistic wavebreaking field $E_p=m_ec^2k_p/e$=11.4 GV/m, where $k_p=2\pi/\lambda_p$. The fields exceed E_p, showing that they are nonlinear, with a peak value of -16.5 GV/m.

Fig. 4d. This lineout of E_z along r=0 shows more clearly the periodicity and the peak values. The magnitude of the peak values decreases with distance from the electron beam, corresponding to a loss of coherence in the plasma wake over time.

Fig. 5a. Given a pre-ionized plasma density of $1.4\text{x}10^{16}$ cm^{-3} and a neutral Li density of $1.26\text{x}10^{17}$ cm^{-3}, the

plasma wake is severely disrupted. The spatial dimensions are normalized to λ_p=89 μm, corresponding to a total plasma density n_e=1.4x10^{17} cm^{-3}. The pre-ionized plasma is represented by seven particles per cell. Up to 27 Li^+/e^- pairs are created in each cell where tunneling ionization of the neutral Li occurs.

Fig. 5b. This lineout of the longitudinal electric field E_z along r=0 shows periodicity with wavelength λ_p, corresponding to the total plasma density of 1.4x10^{17} cm^{-3}. The field is normalized to the cold, nonrelativistic wavebreaking field E_p=36.1 GV/m. The fields do not exceed E_p, showing a linear plasma response.

Fig. 6a. Given a neutral Li density of 1.4x10^{16} cm^{-3} with no pre-ionized plasma, the plasma wake generated by the ionized electrons is incoherent. The driving e^- beam has the same parameters as shown in Fig. 4a above. Up to 27 Li^+/e^- pairs are created in each cell where tunneling ionization of the neutral Li occurs.

Fig. 6b. This lineout of the longitudinal electric field E_z along r=0 shows that the incoherent wake seen in Fig. 6a cannot sustain large electric fields. The field is normalized to the cold, nonrelativistic wavebreaking field E_p=11.4 GV/m. The fields do not exceed E_p, showing a linear plasma response.

Fig. 7a. The nonlinear plasma wake, driven by the self-fields of a shorter, narrower 50 GeV e^- drive beam, becomes completely decoherent in just two plasma wavelengths. Up to 27 Li^+/e^- pairs are created in each cell where tunneling ionization of the neutral Li occurs.

Fig. 7b. This lineout of E_z along r=0 shows the peak values decrease rapidly with distance from the electron beam. The field is normalized to the cold, nonrelativistic wavebreaking field E_p=11.4 GV/m. The fields exceed E_p, showing an initially nonlinear plasma response.

XIII. FIGURES

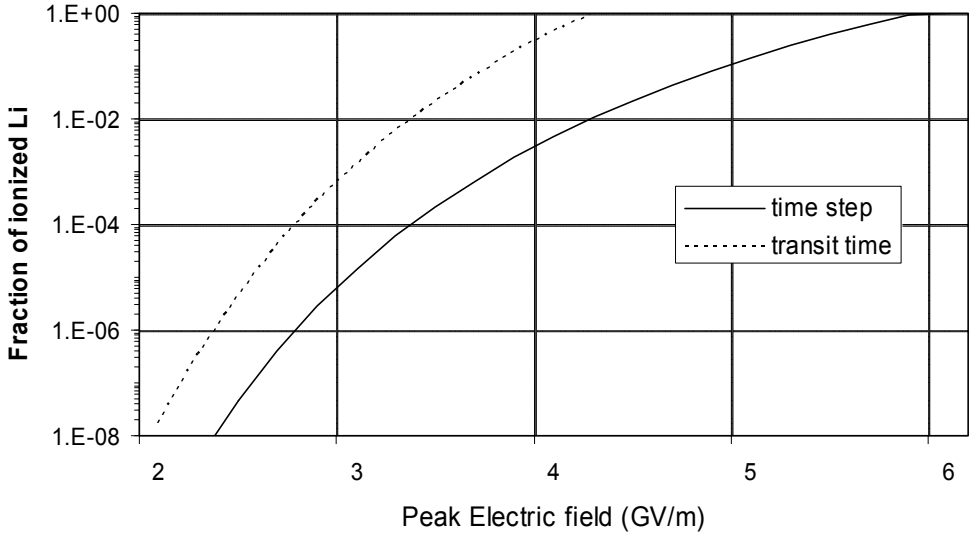

Figure 1.

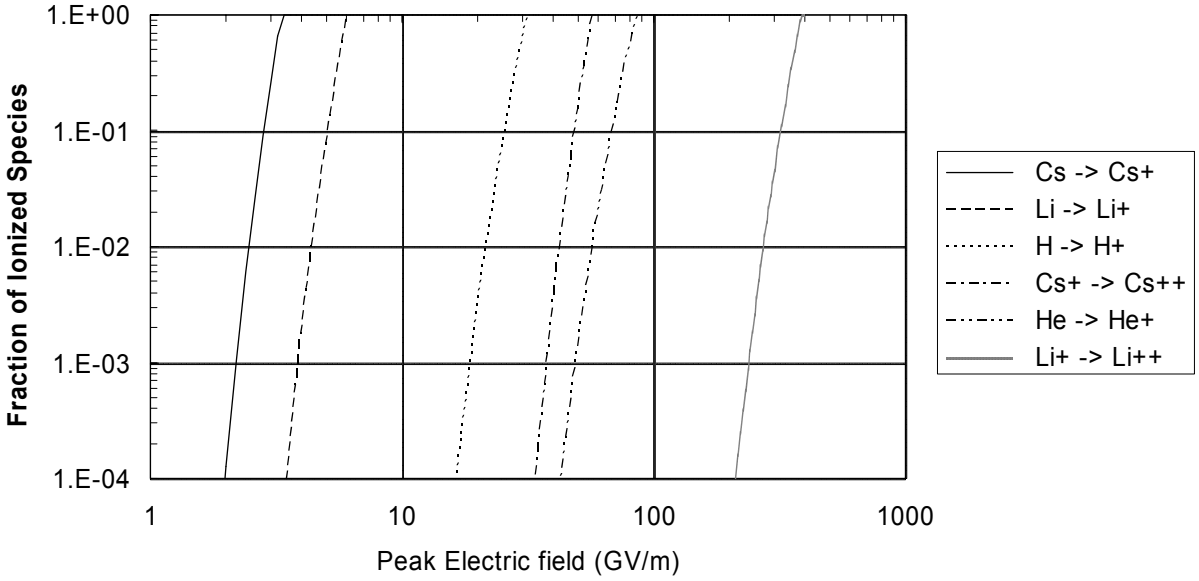

Figure 2.

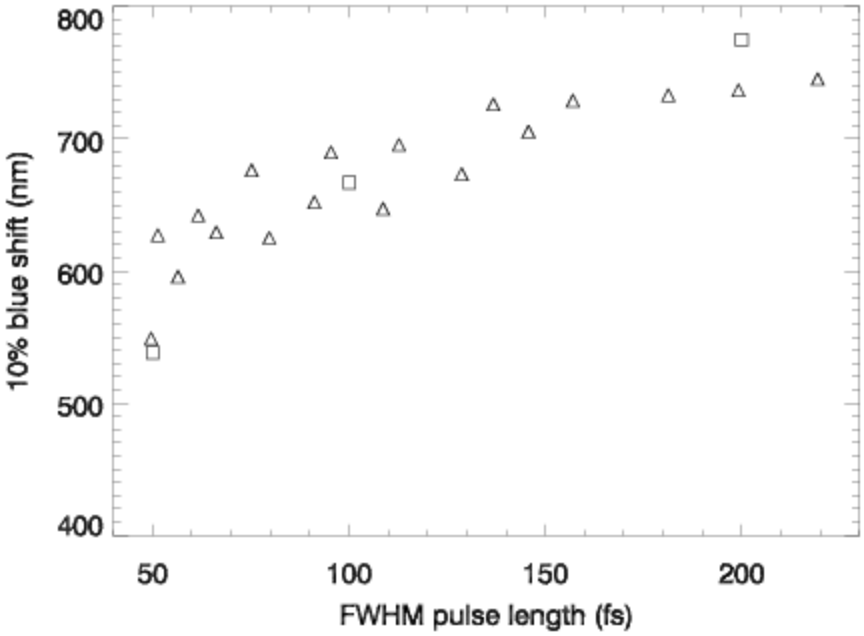

Figure 3.

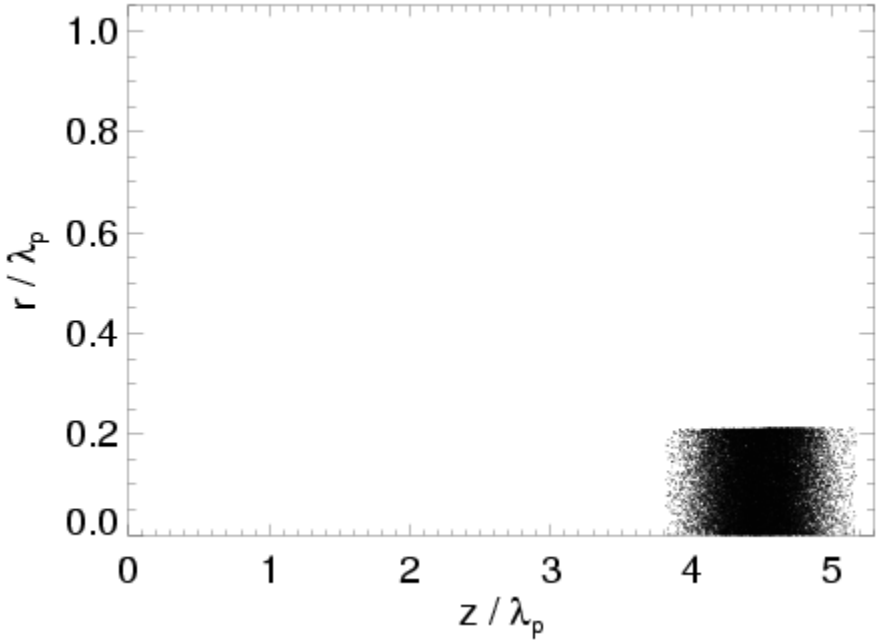

Figure 4a.

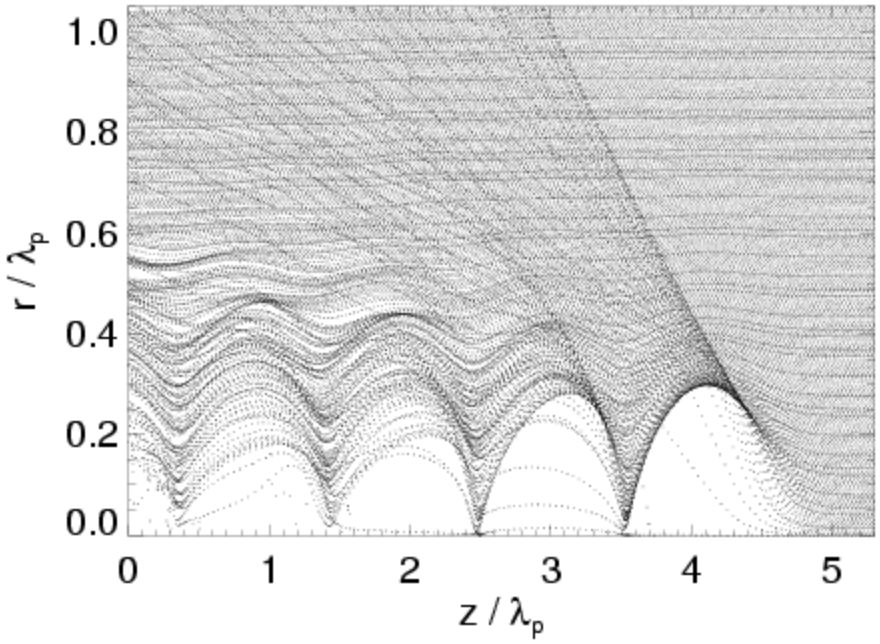

Figure 4b.

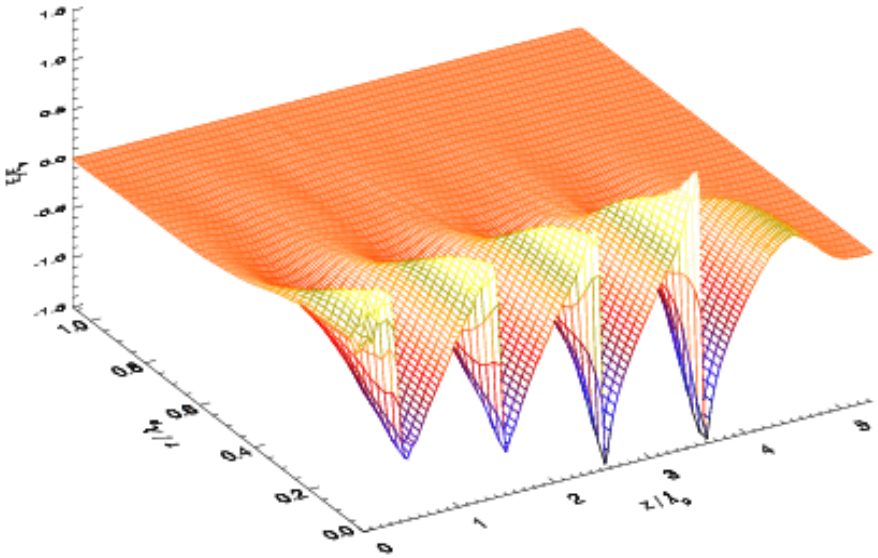

Figure 4c.

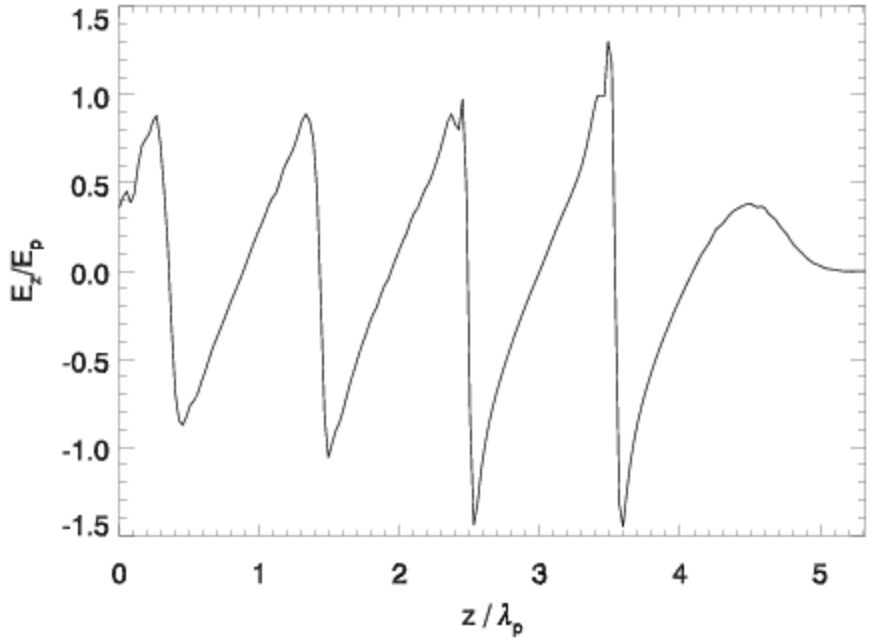

Figure 4d.

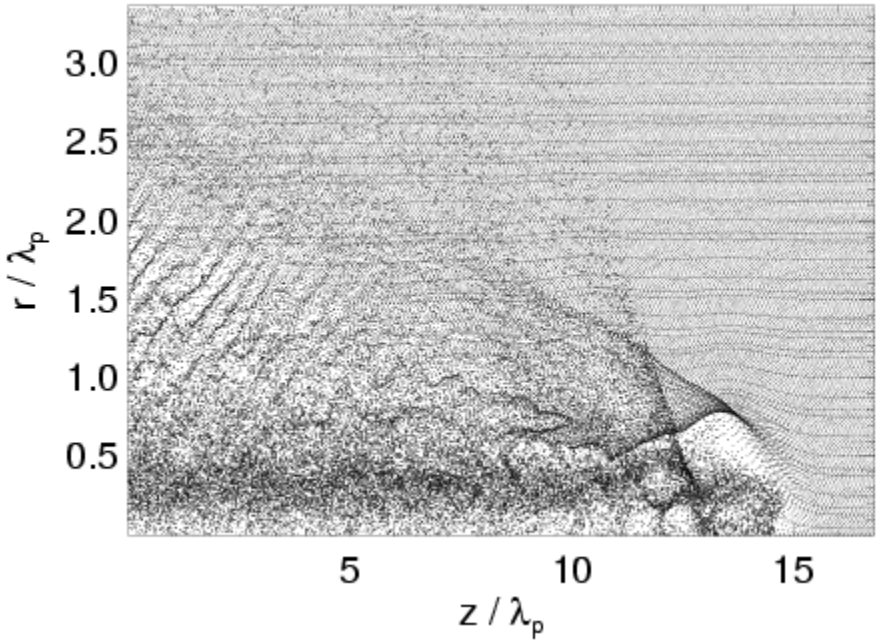

Figure 5a.

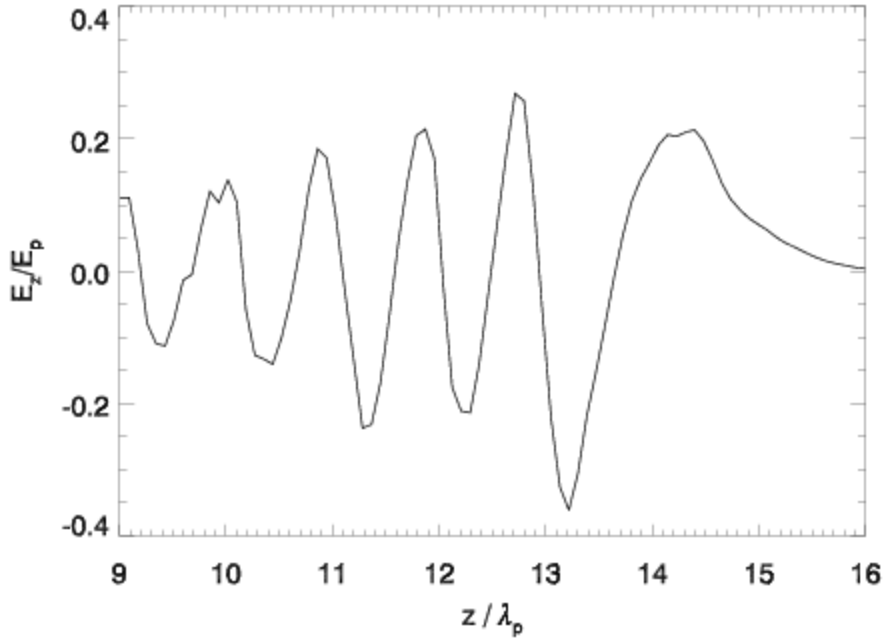

Figure 5b.

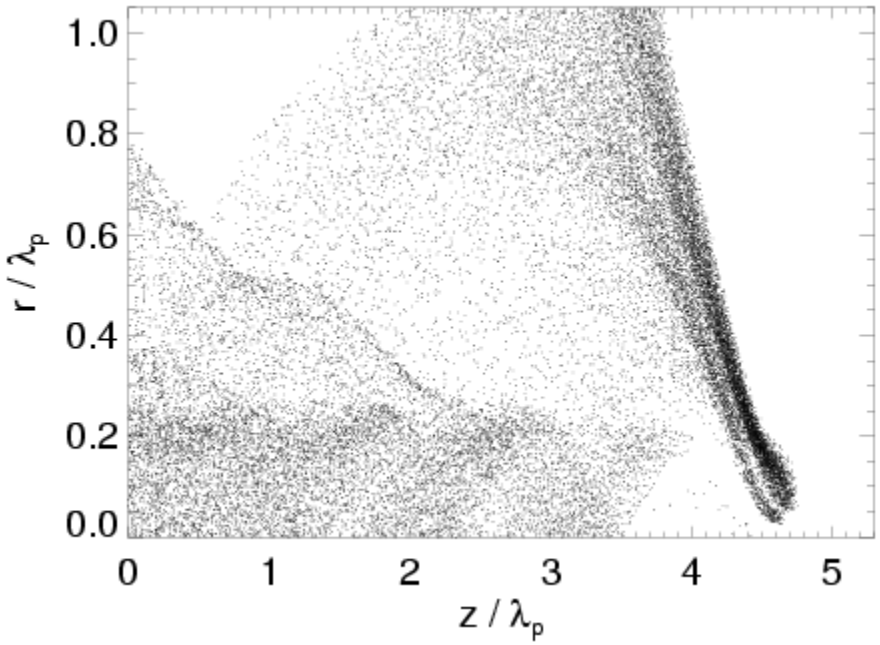

Figure 6a.

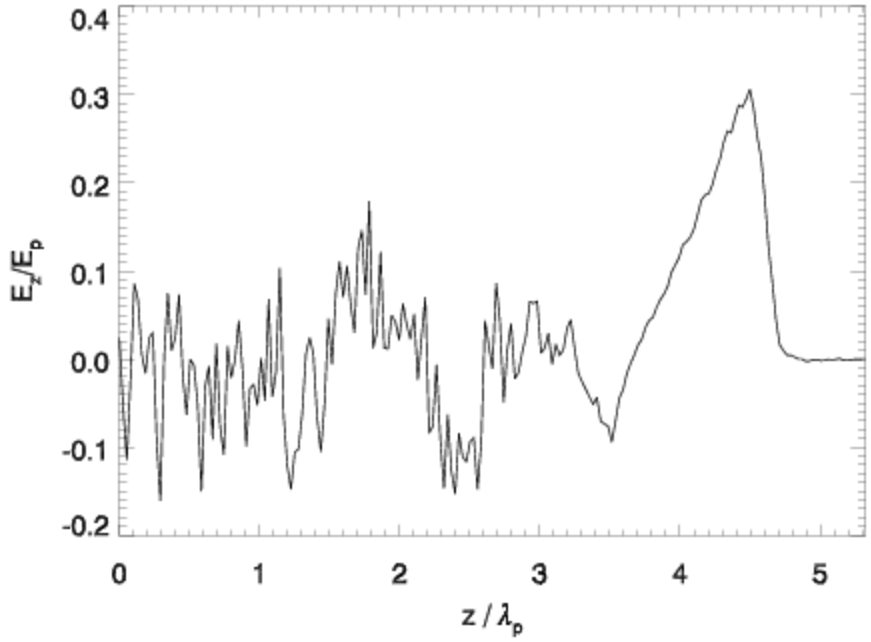

Figure 6b.

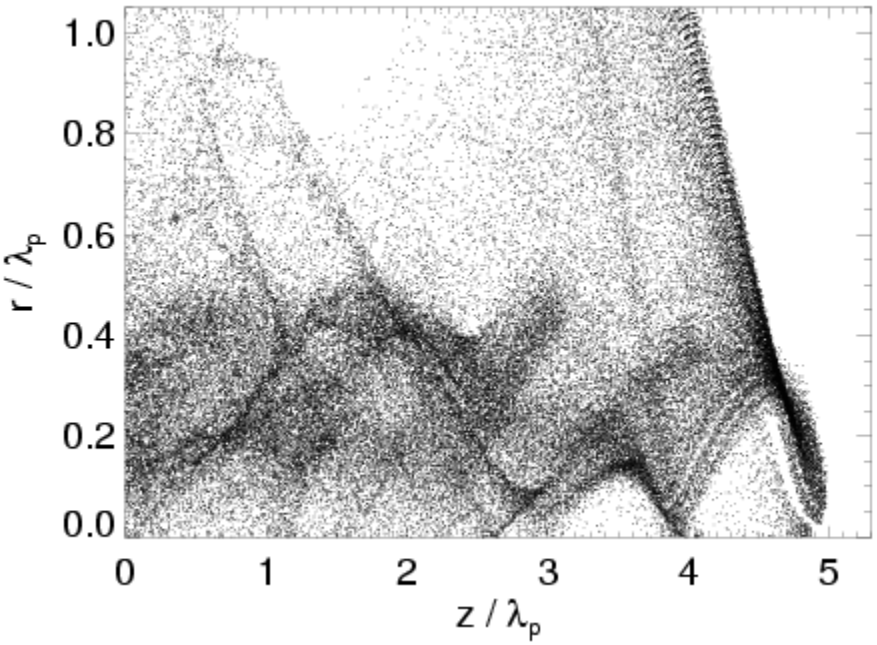

Figure 7a.

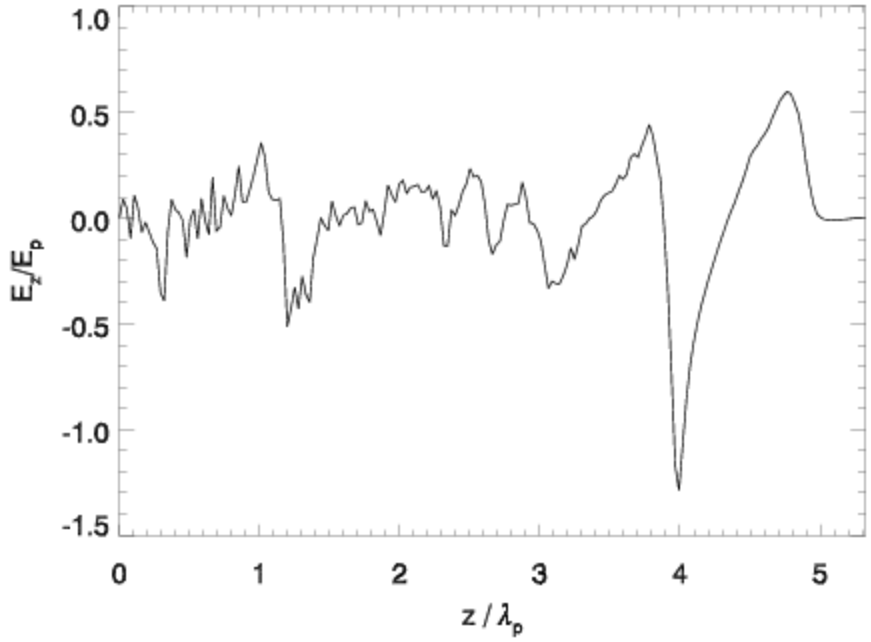

Figure 7b.